Quantum lattice dynamical effects on single-particle excitations in one-dimensional Mott and Peierls insulators

H. Fehske,[1] G. Wellein,[2] G. Hager,[2] A. Weiße,[3] and A. R. Bishop[4]

[1]*Institut für Physik, Ernst-Moritz-Arndt Universität Greifswald, D-17487 Greifswald, Germany*

[2]*Regionales Rechenzentrum Erlangen, Universität Erlangen, D-91058 Erlangen, Germany*

[3]*School of Physics, The University of New South Wales, Sydney, New South Wales 2052, Australia*

[4]*Theoretical Division and Center for Nonlinear Studies, Los Alamos National Laboratory, Los Alamos, New Mexico 87545, USA*

As a generic model describing quasi-one-dimensional Mott and Peierls insulators, we investigate the Holstein-Hubbard model for half-filled bands using numerical techniques. Combining Lanczos diagonalization with Chebyshev moment expansion we calculate exactly the photoemission and inverse photoemission spectra, and use these to establish the phase diagram of the model. While polaronic features emerge only at strong electron-phonon couplings, pronounced phonon signatures, such as multiquanta band states, can be found in the Mott insulating regime as well. In order to corroborate the Mott to Peierls transition scenario, we determine the spin- and charge-excitation gaps by a finite-size scaling analysis based on density-matrix renormalization-group calculations.

The one-dimensional (1D) Holstein-Hubbard model (HHM) has been used extensively to describe for low-dimensional materials, e.g., conjugated polymers, organic charge transfer salts, or halogen-bridged transition metal complexes,[1] and the associated metal-insulator[2,3] and insulator-insulator transitions.[4–6] The HHM accounts for a tight-binding electron band, intrasite Coulomb repulsion between electrons of opposite spin, and a local coupling of the charge carriers to the phonon system:

$$H = -t\sum_{i,\sigma} (c_{i\sigma}^\dagger c_{i+1\sigma} + \text{H.c.}) + U\sum_i n_{i\uparrow}n_{i\downarrow}$$

$$- \sqrt{\varepsilon_p \omega_0}\sum_{i,\sigma} (b_i^\dagger + b_i)n_{i\sigma} + \omega_0\sum_i b_i^\dagger b_i. \quad (1)$$

Here, $c_{i\sigma}^\dagger$ ($c_{i\sigma}$) denote fermionic creation (annihilation) operators of spin-σ electrons ($\sigma = \uparrow, \downarrow$) on a 1D lattice with N sites, $n_{i\sigma} = c_{i\sigma}^\dagger c_{i\sigma}$, and $b_i^\dagger$ (b_i) are the corresponding bosonic operators for a dispersionless optical phonon with frequency ω_0.

The physics of the model (1) is governed by the competition between electron itinerancy ($\propto W = 4t$) on the one hand and electron-electron ($\propto u = U/4t$) and electron-phonon ($\propto \lambda = \varepsilon_p/2t$; ε_p is the polaron shift) interactions on the other hand, which both tend to immobilize the charge carriers. At least for the half-filled band case ($\Sigma_{i,\sigma}n_{i\sigma} = N_{el} = N$), Mott insulator (MI) or Peierls insulator (PI) states are expected to be favored over the metallic state at temperature $T = 0$ (see Fig. 1). The correlated MI shows pronounced spin-density-wave (SDW) fluctuations but has continuous symmetry. It therefore exhibits no long-range order in 1D. In contrast, the PI is characterized by dominant charge-density-wave (CDW) correlations and true long-range order because a discrete symmetry is broken. While the gaps to both spin (Δ_s) and charge (Δ_c) excitations are finite in the PI, the spin gap vanishes in the 1D MI, which is related to spin charge separation. In a strict sense these results hold in the adiabatic

limit ($\omega_0 = 0$) for "U-only" (Hubbard model) and "λ-only" (Peierls model) parameters. At finite phonon frequency and $U = 0$ (Holstein model) a critical electron-phonon (EP) coupling is required to set up the CDW phase characterized by alternating doubly occupied and empty sites.[7] The concomitant gap formation and metal-insulator transition have recently been studied in the limit of infinite dimensions.[8] Depending on the adiabaticity ratio $\alpha = \omega_0/t$ the PI represents a traditional band insulator ($\alpha \ll 1$) or a bipolaronic insulator ($\alpha \gg 1$, $g^2 = \varepsilon_p/\omega_0 \gg 1$).[9] Although for the more general HHM the situation is much less clear, we expect that the features of the insulating phase will depend markedly on the ratio of Coulomb and EP interactions u/λ, allowing for quantum phase transitions between insulating phases. Indeed, based on recent numerical results for the staggered spin- and charge-structure factors, it has been argued that the HHM shows a crossover between Mott and Peierls insulating
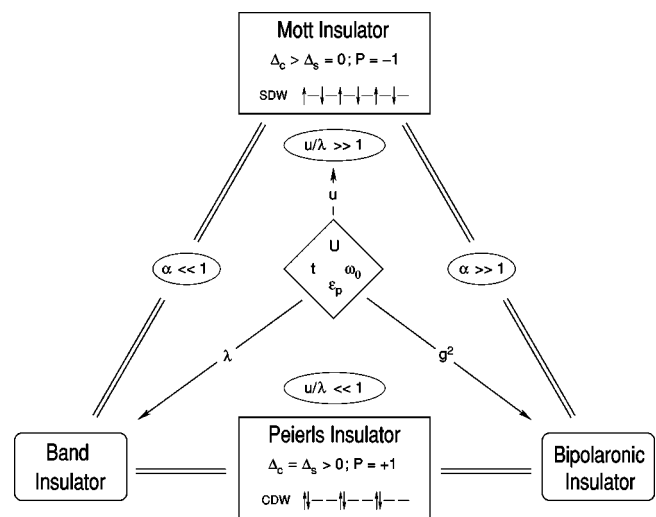

FIG. 1. Schematic phase diagram of the Holstein-Hubbard model at half filling.

phases at $u/\lambda \simeq 1$.[10] More precisely, for finite periodic chains, the MI-PI quantum phase transition could be identified by a ground-state level crossing associated with a change in the parity eigenvalue P.[4] Note that this scenario differs from the (weakly interacting) HHM with frozen phonons,[10] where there is strong evidence in favor of two quantum critical points, as in the ionic Hubbard model.[11,12]

The aim of this work is to establish the physical picture developed to date for the interplay of spin, charge, and lattice degrees of freedom in the 1D Holstein Hubbard model. In particular, we attempt to verify the proposed phase diagram by examining the single-particle excitations. For these purposes we employ Lanczos exact diagonalization (ED),[13] kernel polynomial,[14] and density-matrix renormalization group (DMRG)[15,16] methods to determine the (inverse) photoemission spectra as well as the spin- and charge-excitation gaps. These quasi-exact numerical techniques allow us to obtain reliable results for all interaction strengths with the full quantum dynamics of phonons taken into account. Exact diagonalizations are seriously limited in achievable system sizes N, but have the advantage that spectral quantities are easily accessible. Complementary, the DMRG algorithm yields specific eigenstates of large systems by implementing a renormalization scheme and an optimal truncation of the Hilbert space. Thus it permits for a finite-size analysis of the ground-state energies in different particle and spin sectors, which is required to determine the behavior of the various excitation gaps in the thermodynamic limit.

We begin by studying the spectral density of single-particle excitations associated with the injection of a spin-σ electron with wave number K, $A_{K\sigma}^+(\omega)$ [inverse photoemission (IPE)], and the corresponding quantity for the emission of an electron, $A_{K\sigma}^-(\omega)$ [photoemission (PE)], where

$$A_{K\sigma}^\pm(\omega) = \sum_m |\langle \psi_m^{(N_{el}\pm 1)}|c_{K\sigma}^\pm|\psi_0^{(N_{el})}\rangle|^2$$

$$\times \delta[\omega \mp (E_m^{(N_{el}\pm 1)} - E_0^{(N_{el})})] \qquad (2)$$

with $c_{K\sigma}^+ = c_{K\sigma}^\dagger$ and $c_{K\sigma}^- = c_{K\sigma}$. $|\psi_0^{(N_{el})}\rangle$ is the ground state of the system with N_{el} electrons and $|\psi_m^{(N_{el}\pm 1)}\rangle$ are eigenstates of the $(N_{el}\pm 1)$-particle system. $E_0^{(N_{el})}$ and $E_m^{(N_{el}\pm 1)}$ are the corresponding energies. Adding the spectral densities of (photo) emission and absorption we obtain the spectral function $A_{K\sigma}(\omega) = A_{K\sigma}^+(\omega) + A_{K\sigma}^-(\omega)$, which obeys various sum rules and allows for a connection to angle-resolved photoemission spectroscopy (ARPES). The simplest sum rule, $\int_{-\infty}^{\infty} A_{K\sigma}(\omega)d\omega = 1$, reflects the normalization of $A_{K\sigma}(\omega)$ but is not useful for ARPES since it involves both occupied and unoccupied states. $\Sigma_\sigma \int_{-\infty}^{\infty} n_F(\omega)A_{K\sigma}(\omega)d\omega = n(K)$ [where $n_F(\omega)$ is the Fermi function] is more important, since it relates the ARPES intensity to the number of electrons in a momentum state K: $n(K) = \Sigma_\sigma \langle c_{K\sigma}^\dagger c_{K\sigma}\rangle$. The ED results presented for $A_{K\sigma}^\pm(\omega)$ in the following were obtained for an eight-site system with periodic boundary conditions.[17]

Let us first consider the MI regime. Figure 2 displays the IPE and PE spectra for the HHM at the allowed wave numbers of our finite system: $K = 0, \pm\pi/4, \pm\pi/2, \pm 3\pi/4$, and π.
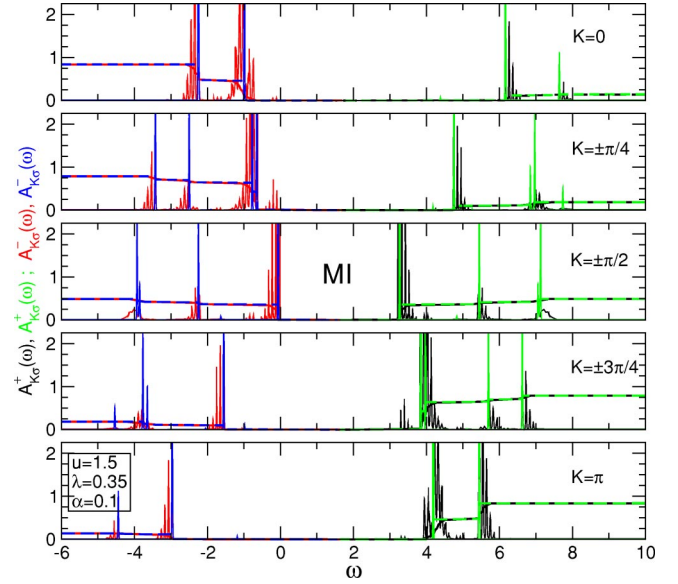

FIG. 2. (Color online) Wave-number-resolved spectral densities for photoemission [$A_{K\sigma}^-(\omega)$; red lines (left)] and inverse photoemission [$A_{K\sigma}^+(\omega)$; black lines (right)] in the Mott insulating state ($u/\lambda \gg 1$). The corresponding integrated densities $S_{K\sigma}^\pm(\omega)$ are given by dashed lines. Data for the pure Hubbard model (blue and green lines) were shifted by $-(\varepsilon_p N_{el}^2/N)$ and included for comparison.

To reliably monitor a possible band splitting induced by the Hubbard and EP couplings at half filling it is necessary to guarantee that the Fermi momenta $K_F = \pm\pi/2$ are occupied, which is the case for $N = 4l$ (l integer, periodic boundary conditions). The most prominent feature we observe in the MI regime is the opening of a gap at $K = \pm\pi/2$, indicating massive charge excitations. A comparison with the results obtained for the pure Hubbard model classifies this gap as the Mott-Hubbard correlation gap. Its value $\Delta/t \simeq 3.25$ almost coincides with the optical gap Δ_{opt} we determined by evaluating the regular part of the optical conductivity for the same parameters. The dispersion of the lower (upper) Hubbard band can be derived tracing the uppermost (lowest) excitations in each K sector. Due to the finiteness of our system and the rather moderate value $u = 1.5$, PE (IPE) excitations with $K = \pm 3\pi/4$ and π ($K = \pm\pi/4$ and 0) have still finite spectral weight. This can be seen from the integrated spectral densities $S_{K\sigma}^\pm(\omega) = \int_{\mp\infty}^{\omega} d\omega' A_{K\sigma}^\pm(\omega')$, which, in addition to the sum rule $S_{K\sigma}^-(-\infty) + S_{K\sigma}^+(\infty) = 1$, satisfy the relations $S_{K\sigma}^\pm(\pm\infty) + S_{\pi-K\sigma}^-(\pm\infty) = 1$ ($K \geq 0$). Since the spectral weight of the PE excitations with $K > \pi/2$ is expected to vanish as N goes to infinity for $u \gg 1$, the lower Hubbard band will be completely filled [$\Sigma_{|K| \leq K_F, \sigma} \int_{-\infty}^{-\infty} d\omega A_{K\sigma}^-(\omega) \simeq N_{el}$], and consequently the system behaves as an insulator at $T = 0$.[20] As a result of the coupling to the phonon system the electronic levels in each K sector split, creating phonon side bands. The distinct peaks are separated by multiples of the bare phonon frequency and can be assigned to relaxation processes of the $Q = 0$ phonon modes.[21] The number of phonons involved is controlled by g^2. $S_{K\sigma}^\pm(\omega)$ shows clearly that the total spectral weight of the resulting excitation bands equals the weight of the respective electronic excitations in
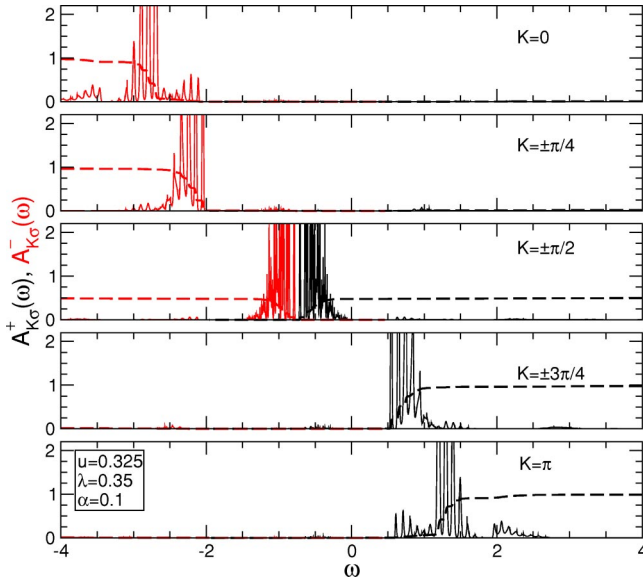
FIG. 3. (Color online) PE [red lines (left)] and IPE [black lines (right)] spectra near the Mott insulator Peierls insulator transition point ($u \simeq \lambda$).

the pure Hubbard model. Interestingly, mediated by $Q \neq 0$ phonons, there appear "shadows" of the band belonging to a dominant electronic excitation in a certain K sector in other K sectors, giving rise to a weak "breather-like" excitation,[22] which is almost dispersionsless in the Brillouin zone.

If we decrease the Hubbard interaction at fixed EP coupling strength the Mott-Hubbard gap weakens and finally closes at about $(u/\lambda)_c \simeq 1$, which marks the MI-PI crossover. This is the situation shown in Fig. 3. Approaching the critical point from above and below, the ground state and the first-excited state become degenerate. These states have different eigenvalues P of the site-inversion operator $P c_{i\sigma}^{\dagger} P^{\dagger} = c_{N-i\ \sigma}^{\dagger}$ ($i = 0, \ldots, N-1$) and we have verified that the ground-state site parity is $P = +1$ in the MI and $P = -1$ in the PI. Obviously the critical point is characterized by gapless charge excitations at the Fermi momenta but should not be considered as metallic because the Drude weight is ill defined.[11,23]

If the Hubbard interaction is further reduced, i.e., the EP coupling overcomes the on-site Coulomb repulsion, a CDW accompanied by a dimerization of the lattice develops. As a result the electronic band structure becomes gapped again [see Fig. 4 (upper panel)]. The form of the spectra, however, is quite different from MI case. While in the MI regime the lowest peak in each K sector is clearly the dominant one, in the BI phase rather broad (I)PE signatures appear. Within these excitation bands the spectral weight is almost uniformly distributed, which is a clear signature of multiphonon absorption and emission processes that accompany every single-particle excitations in the PI. The line shape then reflects the (Poisson-like) distribution of the phonons in the ground state. Again low-intensity "shadow bands" become visible. Remarkably, now the cumulative spectral weight $\Sigma_{|K| \leq \pi/2} S_{K\sigma}^{-}(-\infty)$ gives nearly the total number N_{el} of elec-
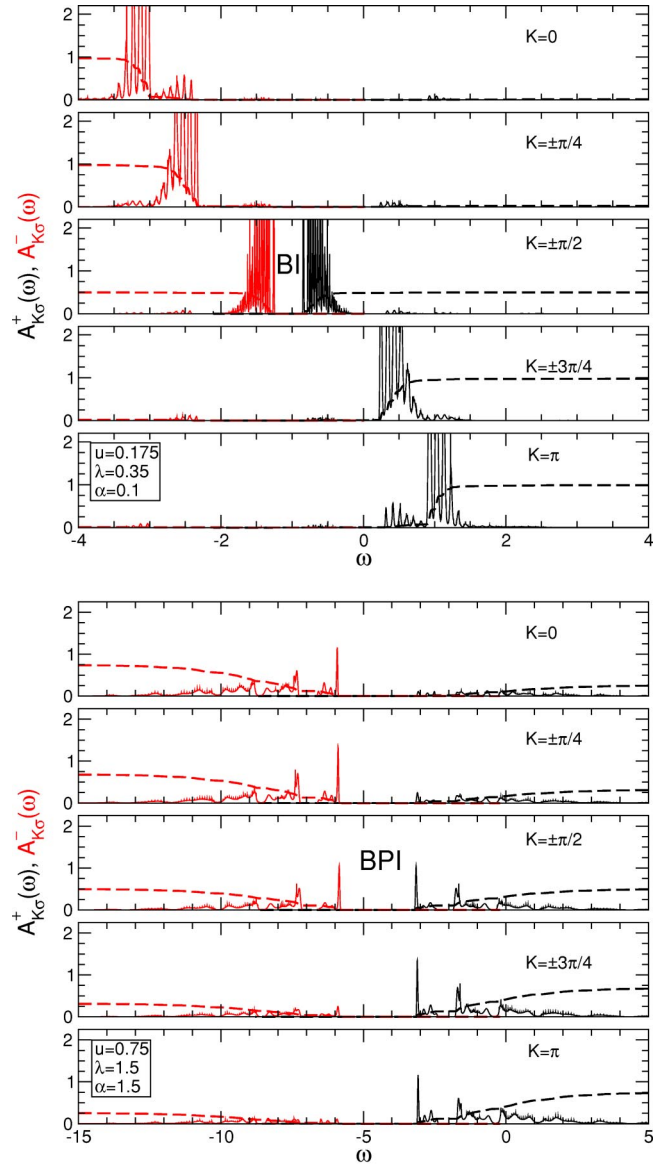

FIG. 4. (Color online) PE and IPE spectra in the Peierls phase ($u \ll \lambda$). The upper (lower) panels show typical results obtained for the case of a band insulator (BI) at $\alpha \ll 1$ and bipolaronic insulator (BPI) at $\alpha \gg 1$, respectively.

trons, i.e., the finite-size effects mentioned above for the MI are much less pronounced in the BI state. The situation changes radically if the insulating behavior is associated with localized bipolarons forming a CDW state (see Fig. 4, lower panel). Due to strong polaronic effects an almost flat band dispersion results with exponentially small (electronic) quasiparticle weight. Now the dominant peaks in the incoherent part of the (I)PE spectra are related to multiples of the (large) bare phonon frequency broadened by electronic excitations.

Since many-body gaps to excited states form the basis for making contact with experimentally measurable excitation gaps and can also be used to characterize different phases of the HHM, we finally determine the charge and spin gaps,
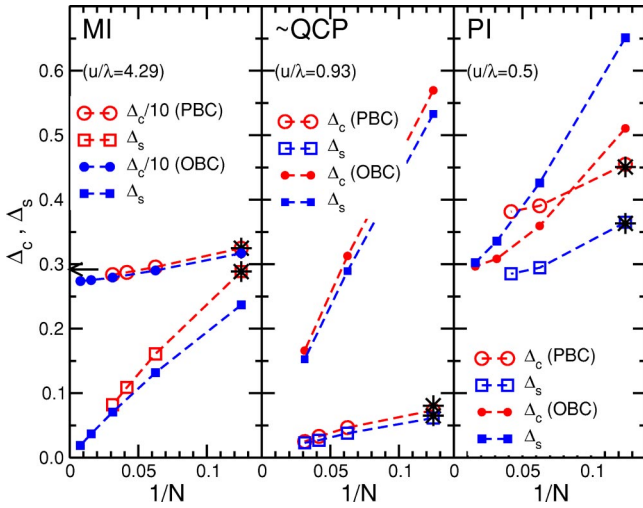
FIG. 5. (Color online) DMRG finite-size scaling of spin- and charge-excitation gaps in the HHM with dynamical phonons ($\lambda = 0.35$, $\alpha = 0.1$). Note the different scale of Δ_c in the MI phase. Open and filled symbols denote DMRG results for periodic (PBC) and open (OBC) boundary conditions, respectively. The accessible system sizes are smaller at larger λ/u, where an increasing number of (phononic) pseudosites is required to reach convergence with respect to the phonons. Stars represent the ED results for the eight-site system. The arrow marks the value of the optical gap Δ_{opt} for the Bethe-ansatz solvable 1D Hubbard model, which is given by $\Delta_{opt}/4t = u - 1 + \ln(2)/2u$ in the limit of large $u > 1$ (Ref. 24).

$$\Delta_c = E_0^{(N+1)}(\tfrac{1}{2}) + E_0^{(N-1)}(-\tfrac{1}{2}) - 2E_0^{(N)}(0), \quad (3)$$

$$\Delta_s = E_0^{(N)}(1) - E_0^{(N)}(0), \quad (4)$$

using DMRG.[18] Here $E_0^{(M)}(S^z)$ is the ground-state energy of the HHM with M particles in the sector with total spin-z component S^z.

Obviously the finite-size scaling presented in Fig. 5 for $\Delta_{c/s}$ substantiates our introductory discussion of the phase diagram (cf. Fig. 1). Δ_c and Δ_s are finite in the PI and will converge further as $N \to \infty$. Both gaps seem to vanish at the quantum phase transition point of the HHM with finite-frequency phonons, but in the critical region the finite-size scaling is extremely delicate. In the MI we found a finite charge excitation gap, which in the limit $u/\lambda \gg 1$ scales to the optical gap of the Hubbard model, whereas the extrapolated spin gap remains zero.[19]

In summary, we have presented a comprehensive picture of the physical properties of the 1D half-filled finite-phonon frequency Holstein-Hubbard model. With respect to the metal the electron-electron coupling favors the Mott insulating state whereas the electron-phonon interaction is responsible for the Peierls insulator to occur. The PI typifies a band insulator in the adiabatic weak-to-intermediate coupling range or a bipolaronic insulator for non-to-antiadiabatic strong coupling. Our results for the single-particle spectra and spin/charge excitation gaps give clear indication of a Mott- to Peierls-insulator quantum phase transition at $u/\lambda \simeq 1$. Quantum phonon dynamics yields pronounced effects in the (I)PE spectra, which might be of great importance for interpreting photoemission experiments of low-dimensional strongly correlated electron-phonon systems such as MX-chain compounds.[1]

[1] N. Tsuda, K. Nasu, A. Yanese, K. Siratori, *Electronic Conduction in Oxides* (Springer-Verlag, Berlin, 1990); A.R. Bishop and B.I. Swanson, Los Alamos Sci. **21**, 133 (1993); *Organic Conductors*, edited by J.-P. Farges (Marcel Dekker, New York, 1994).

[2] N. Mott, *Metal-Insulator Transitions* (Taylor & Francis, London, 1974); R. Peierls, *Quantum Theory of Solids* (Oxford University Press, Oxford, 1955).

[3] M. Capone, G. Sangiovanni, C. Castellani, C. Di Castro, and M. Grilli, Phys. Rev. Lett. **92**, 106401 (2004).

[4] H. Fehske, G. Wellein, A. Weiße, F. Göhmann, H. Büttner, and A.R. Bishop, Physica B **312-313**, 562 (2002).

[5] P. Sengupta, A.W. Sandvik, and D.K. Campbell, Phys. Rev. B **67**, 245103 (2003).

[6] The 2D case has been studied in E. Berger, P. Valášek, and W. von der Linden, Phys. Rev. B **52**, 4806 (1995).

[7] R.J. Bursill, R.H. McKenzie, and C.J. Hamer, Phys. Rev. Lett. **80**, 5607 (1998); E. Jeckelmann, C. Zhang, and S.R. White, Phys. Rev. B **60**, 7950 (1999); H. Fehske, M. Holicki, and A. Weiße, Adv. Solid State Phys. **40**, 235 (2000).

[8] D. Meyer, A.C. Hewson, and R. Bulla, Phys. Rev. Lett. **89**, 196401 (2002); M. Capone and S. Ciuchi, Phys. Rev. Lett. **91**, 186405 (2003).

[9] In the antiadiabatic limit $\omega_0 = \infty$, where the lattice reacts instantaneously to the electronic configuration, an effective (nonretarded) attractive Hubbard model results.

[10] H. Fehske, A.P. Kampf, M. Sekania, and G. Wellein, Eur. Phys. J. B **31**, 11 (2003).

[11] A.P. Kampf, G.I. Japradize, M. Sekania, and Ph. Brune, J. Phys.: Condens. Matter **15**, 5895 (2003).

[12] S.R. Manmana, V. Meden, R.M. Noack, and K. Schönhammer, arXiv:cond-mat/0307741 (unpublished); C.D. Batista and A.A. Aligia, arXiv:cond-mat/0309295 (unpublished).

[13] J.K. Cullum and R.A. Willoughby, *Lanczos Algorithms for Large Symmetric Eigenvalue Computations* (Birkhäuser, Boston, 1985), Vols. I and II; G. Wellein, H. Röder, and H. Fehske, Phys. Rev. B **53**, 9666 (1996).

[14] R.N. Silver and H. Röder, Phys. Rev. E **56**, 4822 (1997); B. Bäuml, G. Wellein and H. Fehske, Phys. Rev. B **58**, 3663 (1998).

[15] S.R. White, Phys. Rev. Lett. **69**, 2863 (1992).

[16] G. Hager, E. Jeckelmann, H. Fehske, and G. Wellein, J. Comput. Phys. **194**(2), 795 (2004).

[17] In the ED calculations we separate the $Q=0$ phonon mode (with an average occupation number of g^2 per site for the half-filled case) and restrict ourselves to states with a maximum number of M phonons for $N-1$ phonon modes. We achieve good convergence for $M=22$ even in the PI regime but the use of leading-edge supercomputers is still mandatory to handle the resulting Hamilton matrices with dimensions of 7×10^9. The effect of the $Q=0$ phonon mode in the (I) PE spectra can be easily calculated and, of course, is included in the data shown.

[18] All DMRG calculations were done with $m=1000$ and $n_b=2$, 3 or 4 phonon pseudosites in the MI, QCP, and PI regimes, respectively. The low number of pseudosites was made possible by performing a linear shift $-g\omega_0 N_{el}/N$ of the on-site potentials, which effectively removes the $Q=0$ phonon mode. For comparision with ED data, the number of "real" phonon states is 2^{n_b} (Ref. 16). Computational Resources ranged up to 10 GB of memory and 250 CPU hours on a current Itanium 2 machine (SGI Altix) for the 128-site PI cases.

[19] The ground-state calculation in the MI case with PBC shows a peculiar behavior when going beyond 32 sites. At 64 sites and larger it coincides exactly with the OPC ground state, showing a vanishing bond order at site 64. PBC are hard to establish in our algorithm because of the particular way the DMRG sweeps are performed. Modifications which do not show these deficiencies are under investigation.

[20] Compare the QMC data obtained for the pure Hubbard model in R. Preuss, A. Muramatsu, W. von der Linden, P. Dietrich, F.F. Assaad, and W. Hanke, Phys. Rev. Lett. **73**, 732 (1994).

[21] These center-of-mass phonon modes are nonorthogonal between sectors containing different numbers of particles; see also J.M. Robin, Phys. Rev. B **56**, 13 634 (1997).

[22] The formation of quantum breathers was proposed by W.Z. Wang, A.R. Bishop, J.T. Gammel, and R.N. Silver, Phys. Rev. Lett. **80**, 3284 (1998).

[23] W. Kohn, Phys. Rev. **133**, A171 (1964).

[24] A.A. Ovchinnikov, Zh. Eksp. Teor. Fiz. **57**, 2137 (1969) [Sov. Phys. JETP **30**, 1160 (1970)]; E. Jeckelmann, F. Gebhard, and F.H.L. Essler, Phys. Rev. Lett. **85**, 3910 (2000).